J. Fluid Mech. (2009), *vol.* 618, *pp.* 361–379.
doi:10.1017/S0022112008004527 Printed in the United Kingdom

Capillary entry pressure and the leakage of gravity currents through a sloping layered permeable rock

ANDREW W. WOODS† AND ADRIAN FARCAS

BP Institute, University of Cambridge, Cambridge CB3 0EZ, UK

(Received 16 March 2008 and in revised form 9 October 2008)

We examine the motion of a buoyant fluid injected into a water-saturated porous rock as it spreads along a thin inclined low-permeability barrier. We account for leakage of the fluid across the barrier once the current is sufficiently deep so that the pressure exceeds the capillary threshold. We show that at some distance from the source, the pressure decreases below this threshold, and all the remaining flux spreads laterally along the barrier. We examine the controls on the partitioning of the flow between the draining flux and the laterally spreading flux and also the controls on the lateral extent of the draining region for the case of an instantaneous release and a maintained release of fluid. We consider the implications of our work for the dispersal of CO_2 plumes which may be sequestered in deep saline aquifers.

1. Introduction

The injection of CO_2 into deep saline aquifers or depleted oil and gas fields has received considerable interest in the context of global warming and the related challenge of reducing anthropogenic carbon emissions into the atmosphere (Kumar *et al.* 2005; Nordbotten, Celia & Bachu 2005). In deep saline aquifers, CO_2 is supercritical and has a density of the order 20 %–40 % smaller than that of water, depending on the temperature and pressure. As a result, there is concern that the CO_2 will migrate through the subsurface and back to human environment, perhaps over time scales of tens to hundreds of years. In order to assess this risk, models are being developed to describe the migration of CO_2 plumes through the subsurface (Hesse *et al.* 2006, 2007; Mitchell & Woods 2006; Vella & Huppert 2006), and data are being collected from various field trials using seismic imaging to interpret the dispersal patterns in the field (Bickle *et al.* 2007). A significant challenge associated with the prediction of such CO_2 transport is the complexity of the subsurface strata through which the CO_2 migrates. This can lead to multiple and tortuous flow paths from the injection point to the surface, with the CO_2 being dispersed laterally over substantial distances but also reaching the surface through different flow paths over a range of different time scales. Data from the Sleipner field in Norway (Bickle *et al.* 2007) has shown that the gas spreads out in a pine tree–type pattern, spreading laterally beneath low-permeability layers while gradually migrating upwards as it leaks through these layers or fractures which cut across the layers.

Some of the models which have been developed to describe the migration of plumes of CO_2 in the subsurface have assessed the buoyancy-driven dispersal through both

† Email address for correspondence: andy@bpi.cam.ac.uk

relatively thin layers (Mitchell & Woods 2006; Nordbotten & Celia 2006), in which the CO_2 plume fills the whole depth of the layer, and deeper layers of permeable rock, in which the CO_2 plume spreads as a relatively thin gravity current (Huppert & Woods 1995; Woods 2002; Hesse *et al.* 2006, 2007). In both cases, the flow is assumed to migrate along an upper impermeable boundary as a thin, laterally extensive flow, and the analysis of the flow dynamics has been based on the assumption of a long, thin current of slowly varying thickness, following the classical work of Bear (1970), Barenblatt, Entov & Ryzhik (1990) and Barenblatt (1996). However, in many cases the overlying layer may not be impermeable but may be of much lower permeability than the main flowing layer. As the CO_2 migrates along the interface between the layers, it may then slowly leak through the low-permeability layer. The permeability of this layer may be associated with the rock itself, or if the layer is pervasively fractured, then on a larger field scale, it may be an effective permeability associated with the fractures (Pritchard 2007). Pritchard, Woods & Hogg (2001) explored the dynamics of a gravity-driven flow migrating along a thin, horizontal low-permeability barrier, accounting for the draining of the flow into the boundary as it spreads along the boundary. Their analysis assumed that the injected fluid was fully miscible with the original fluid in the porous layer and did not account for any inclination of layers towards the horizontal.

Here, we explore the dynamics of the gravity-driven flow of a buoyant fluid as it migrates through a permeable rock, saturated with a second, immiscible fluid, along a thin, inclined low-permeability barrier. We assume that there is a capillary entry pressure which limits the migration of the injected fluid into the seal rock; this arises owing to the effects of the interfacial tension between the injected liquid and the original fluid in the rock which restricts the injected fluid from passing through pore throats into the neighbouring pores (Bear 1970; Dake 1978; Bear & Ryzhik 1998). The magnitude of this capillary entry pressure depends on the interfacial tension between the two fluid phases but has the typical magnitude of 25–50 mN for the CO_2–water system, at temperatures of 0°–100 °C and pressures of the order of 1000 atm (Holloway 2001), but it also depends critically on the pore size. The capillary entry pressure requires the current to have a minimum overpressure before it can drain upwards through the 'seal' layer. Typically, the cross-flow pressure gradient is dominantly hydrostatic, and so this implies that there is a minimum depth of the buoyant layer before it can enter the seal; we refer to this as the capillary depth (cf. Bear 1970). If the depth of the current is greater than this capillary depth, then the injected fluid flows through the thin seal rock and may form a continuous layer across the seal rock. This leakage flow is then driven by the overpressure of the fluid beneath the seal layer (cf. Pritchard *et al.* 2001). However, if, as it is flowing through the seal, the pressure of the injected fluid beneath the seal falls sufficiently, then the interfacial tension may inhibit further flow through the seal layer, and the draining will cease. There may be some hysteresis between the critical pressure required to drive the fluid into the seal layer and the pressure at which the fluid is no longer able to enter the seal layer (cf. Bear 1970; Dake 1978); however, in the present work, for simplicity, we take these to be the same. As a result of the control on the draining exerted by the capillary entry pressure, there is now a nonlinear boundary condition on the dynamics of the spreading current, and we explore the impact of this on the fate of the current. As two limiting cases, in this paper we examine the evolution of the flow arising from both a maintained source of buoyant fluid and an instantaneous finite release of buoyant fluid (cf. Huppert & Woods 1995). Such calculations provide valuable insight into the dispersal process, but they also provide reference solutions

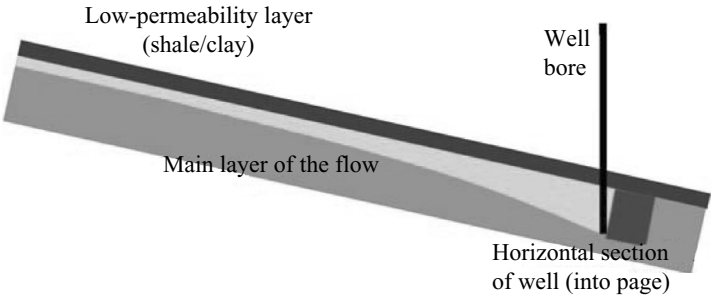

FIGURE 1. Schematic diagram of a generic inclined layer formation and a horizontal injection well, located at the base of the well bore shown in the figure. The horizontal well is directed into the page in the flow layer normal to the slope, so as to produce a two-dimensional current of buoyant fluid which runs upslope as indicated.

for more detailed numerical simulations. We discuss the implications of our model for the dispersal of a CO_2 plume through the subsurface.

2. The buoyant flow along an inclined boundary

If a flux of buoyant fluid issues from a horizontal well beneath an inclined layer of lower permeability, then this layer will act as a vertical barrier to the flow (figure 1). On reaching the boundary, the buoyant fluid will spread along the boundary to form a laterally extensive thin current (cf. Pritchard *et al.* 2001). In this long, thin current, we expect the cross-layer velocity field to be much smaller than the along-layer velocity (cf. Bear 1970; Huppert & Woods 1995), and so the pressure gradient in the cross-layer direction will be approximately given by the hydrostatic pressure in the cross-layer direction, while the along-layer pressure gradient, associated with the along-slope motion, will be balanced by two buoyancy forces. The first one is the along-slope buoyancy force associated with the inclined boundary, and the second one is the buoyancy force associated with the cross-layer component of gravity combined with any change in the depth of the current along the slope (Huppert & Woods 1995). If we denote the thickness of the plume running along the underside of the low-permeability layer to be $h(x, t)$ where $h \ll H$, the thickness of the aquifer, then the cross-layer hydrostatic pressure may be expressed as

$$p(x, y, t) = p_o - \rho_w g \cos\theta(x \tan\theta - h) - \rho_g g \cos\theta(h - y), \tag{2.1}$$

where θ is the angle of the slope to the horizontal; $0 < y < H$ is the downward distance normal to the boundary; x is the distance along the boundary in the upslope direction; p_o is a reference pressure; and ρ_g and ρ_w denote the densities of the injected liquid and the host water (figure 1). The aquifer is assumed to be laterally extensive in the upslope direction, $x > 0$, and for simplicity we therefore examine the motion of the current in the half-plane $x > 0$.

The along-layer motion of the injected fluid in which the buoyancy force drives the flow is given by Darcy's law:

$$u = -\frac{k}{\mu}\left(\frac{\partial p}{\partial x} + \rho_g g \sin\theta\right), \tag{2.2}$$

where k denotes the effective permeability for the motion of the injected fluid as it moves through the main layer of rock below the low-permeability seal. This represents

a useful simplification of the relative permeability in the case of modelling the motion of CO_2 through a water-saturated rock as shown by Nordbotten & Celia (2006) and Hesse *et al.* (2007). Also, μ is the viscosity of the injected fluid, and g the acceleration due to gravity. Local mass conservation requires that the depth of the current varies owing to any gradient of the fluid flux along the boundary together with any draining of fluid through the boundary (cf. Pritchard *et al.* 2001). The cross-layer draining flow is assumed to be driven by the hydrostatic head in the cross-layer direction, $\Delta\rho g\cos\theta(h+b)$, where b is the thickness of the seal layer. In our simplified picture, the injected liquid only enters the seal layer if the cross-layer hydrostatic pressure in the current exceeds the capillary entry pressure into the seal layer, $p_c = \Delta\rho g\cos\theta h_c$, say. Therefore, draining only occurs if $h > h_c$, where $\Delta\rho = \rho_w - \rho_g$. In the limit of a thin seal layer, $h_c \gg b$; then the term $(h+b)$ in the above expression for the cross-layer draining flow can be approximated by h, so that the hydrostatic head driving the cross-layer draining flow can be approximated by the expression $\Delta\rho g\cos\theta h$. In this limit, we also assume that the resistance to flow in the seal exceeds that in the current, $k_u/b \gg k/h_c$, where k_u is the effective permeability of the injected liquid as it moves through the overlying low-permeability 'seal' rock and b is the thickness of the seal rock. The governing equation for the depth of the current then takes the approximate form (cf. Pritchard *et al.* 2001)

$$\phi\frac{\partial h}{\partial t} = \frac{k\Delta\rho g\cos\theta}{\mu}\frac{\partial}{\partial x}\left[h\frac{\partial h}{\partial x} - h\tan\theta\right] - \frac{k_u\Delta\rho g\cos\theta}{\mu b}h \quad \text{for} \quad h \geqslant h_c \tag{2.3}$$

and

$$\phi\frac{\partial h}{\partial t} = \frac{k\Delta\rho g\cos\theta}{\mu}\frac{\partial}{\partial x}\left[h\frac{\partial h}{\partial x} - h\tan\theta\right] \quad \text{for} \quad h < h_c. \tag{2.4}$$

In this model we have assumed that the draining flow of the injected liquid is upward and that there is no downflow of the original formation fluid through the seal layer in response to the upflow. This approximation is motivated by the observation that the speed of the upflow through the seal layer $k_u g\Delta\rho h_c/\mu b$ is greater than the buoyancy-driven exchange flow through the seal layer $k_u g\Delta\rho/mu$ by the factor $h_c/b \gg 1$. Thus any potential Rayleigh–Taylor-type overturn within the seal layer is suppressed by the buoyancy force driving the upflow through the seal, as shown in the analogue Hele-Shaw experiments of Pritchard *et al.* (2001). We have also assumed that the flow front advancing along the inclined slope is planar; physically, this is consistent with the decreasing pressure gradient towards the nose of the flow which results from the increased curvature of the interface at the nose. Experiments reported by Mitchell & Woods (2006), numerical modelling of Nordbotten & Celia (2006) and stability arguments (cf. Mathunjwa & Hogg 2005) are also consistent with the assumption of a planar, non-fingered interface.

In analysing the motion of these draining currents, we consider two limiting problems corresponding to (i) a constant injection rate Q per unit distance across the slope and (ii) an instantaneous release of volume A per unit distance across the slope. For the process of CO_2 sequestration, these limits correspond to the injection phase from a line well and the subsequent gravitational spreading upslope following the injection phase.

3. Constant injection rate

First we focus on the problem of a maintained supply of fluid Q moving upslope from a fixed source; this is a simplification of the more general problem in which

the injected fluid may spread up or down the dip, and we comment further on this in the discussion. The present modelling could in principle represent injection at the apex of a V-shaped impermeable layer or injection upslope of a sealed fault plane intersecting the impermeable layer.

The depth of the current can be scaled by the depth L of a steady current of flux Q migrating along the boundary,

$$L = \frac{\mu Q}{\Delta\rho g \sin\theta k}, \tag{3.1}$$

so that $\hat{h} = h/L$, where the carat denotes a dimensionless variable. We use the draining length of the current as the along-slope scale for the current, noting it is only relevant for that part of the current in which there is draining. This draining length is controlled by the distance the current travels along the slope over the time required to drain into the low-permeability seal. The ratio R of the speed of draining through the seal to the along-slope speed is

$$R = \left(\frac{k_u L \cos\theta}{b}\right)\left(\frac{1}{k \sin\theta}\right), \tag{3.2}$$

where the current thickness, which scales as L, provides the head to drive the fluid through the low-permeability seal of thickness b. Therefore, the draining length is given by

$$X = \frac{k}{k_u} b \tan\theta, \tag{3.3}$$

and we set $\hat{x} = x/X$. The time scale for the draining of the current of thickness L is given as

$$\tau = \frac{\phi b \mu}{k_u \Delta\rho g \cos\theta}, \tag{3.4}$$

so that $\hat{t} = t/\tau$. The dimensionless equations then take the form

$$\frac{\partial \hat{h}}{\partial \hat{t}} = \Gamma \frac{\partial}{\partial \hat{x}}\left(\hat{h}\frac{\partial \hat{h}}{\partial \hat{x}}\right) - \frac{\partial \hat{h}}{\partial \hat{x}} - \hat{h} \quad \text{for} \quad \hat{h} > \hat{h}_c \tag{3.5}$$

and

$$\frac{\partial \hat{h}}{\partial \hat{t}} = \Gamma \frac{\partial}{\partial \hat{x}}\left(\hat{h}\frac{\partial \hat{h}}{\partial \hat{x}}\right) - \frac{\partial \hat{h}}{\partial \hat{x}} \quad \text{for} \quad \hat{h} < \hat{h}_c, \tag{3.6}$$

and the key parameter which emerges from this scaling analysis is

$$\Gamma = \frac{R}{\tan\theta} = \frac{k_u \mu Q}{k^2 b \Delta\rho g \sin\theta \tan^2\theta}, \tag{3.7}$$

where Γ relates the ratio of the speed of draining to the along-slope speed, R, with the gradient of the slope to the horizontal $\tan\theta$. Alternatively, Γ may be interpreted as the ratio of the depth scale of the current advancing along the slope to the length scale required for draining, divided by the gradient of the slope. In solving the dimensionless equations (3.5) and (3.6), we set the flux at $\hat{x} = 0$ to be unity,

$$\Gamma \hat{h}\frac{\partial \hat{h}}{\partial \hat{x}} - \hat{h} = -1, \tag{3.8}$$

and the leading edge of the draining zone, $\hat{x} = \hat{x}_c$, say, is given by the point at which $\hat{h} = \hat{h}_c$. For $\hat{x} > \hat{x}_c$, the depth of the current evolves according to (3.5), and at $\hat{x} = \hat{x}_c$

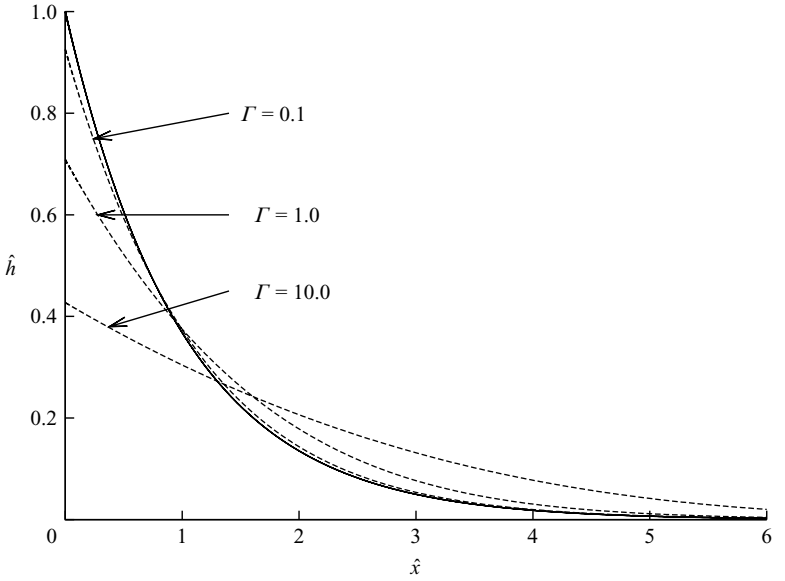

FIGURE 2. Comparison of numerical (— — —) and analytical (—) steady state solutions of the current depth as functions of position from the source for $\Gamma = 0.1,\ 1.0,\ 10.0$.

we require that the current depth and flux be continuous (cf. Pritchard 2007), which requires

$$\left[\hat{h}\right]_{-}^{+} = 0 \quad \text{and} \quad \left[\hat{h}\frac{\partial \hat{h}}{\partial \hat{x}} - \hat{h}\right]_{-}^{+} = 0. \tag{3.9}$$

Finally, at the leading edge of the current, $\hat{h} = 0$. Note that after a finite volume of fluid has been injected, then owing to the nonlinearity, the leading edge of the current extends a finite distance from the source.

3.1. *Steady-state solutions*

We first examine the case $\hat{h}_c = 0$ and then extend the analysis to the case $\hat{h}_c \neq 0$. With $\hat{h}_c = 0$, in the limit $\Gamma \ll 1$ (3.5) has an approximate steady-state solution in which the depth falls to zero exponentially with distance according to

$$\hat{h} \approx \exp(-\hat{x}). \tag{3.10}$$

For larger values of Γ, the structure of the steady solution near the source is nonlinear and requires numerical solution. In figure 2, we compare the steady-state solutions for a range of values of Γ. The figure illustrates how the nonlinear solution converges to the analytical value for small Γ, but for larger Γ, the dimensionless current depth near the source is overpredicted by the linearized model. For small Γ this effect may be seen from an asymptotic expansion of the form $\hat{h}(\hat{x}) \sim h_o(\hat{x}) + \Gamma h_1(\hat{x}) + \cdots$ for which it may be shown from (3.5) that $h_1(\hat{x}) = -2\exp(-2\hat{x})$. Indeed, in figure 3(*a*), we show how the dimensionless current depth at the source decreases with Γ. As Γ increases, one may interpret it as an increase in the depth of the current as it advances upslope or a decrease in the draining length or a decrease in the gradient of the slope (cf. (3.7)); each of these three effects tends to increase the cross-slope spreading which, relative to the scalings for the depth and length, leads to a thinner and longer dimensionless current. Indeed, figure 2 also illustrates how the lateral extent of the current increases

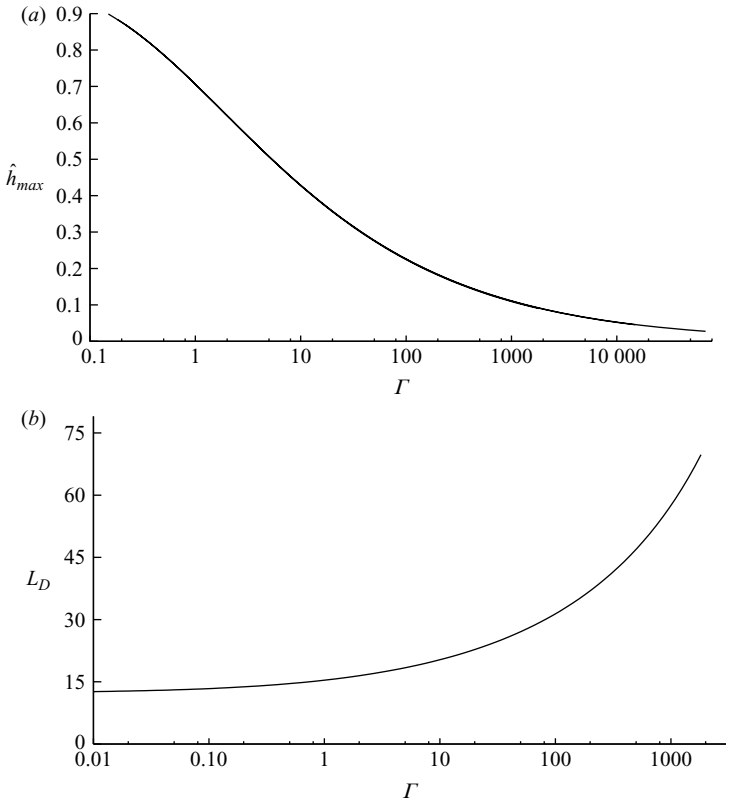

FIGURE 3. Variation with the draining parameter Γ of (*a*) dimensionless depth at the source $\hat{h}_{max}$ and (*b*) the drainage distance L_D defined as the point at which the dimensionless current depth has the value 10^{-6}.

with Γ, and in figure 3(*b*) we illustrate how the dimensionless distance L_D at which the dimensionless current depth has fallen to the value 10^{-6} increases with Γ.

3.2. *Time-dependent motion*

The equations have been solved numerically using a predictor–corrector algorithm (Ames 1977), and the accuracy has been checked to be within 1 % by repeating calculations with one half the time and/or space steps. Figure 4(*a*) illustrates the time evolution of the current as it runs along a low-permeability barrier in the case $\Gamma = 1$. The transient flow adjusts to the steady draining solution shown in figure 2 over a time of order unity. Indeed, further numerical calculations show that the dimensionless time $\hat{t}$ required for the flow to adjust so that the draining flux equals 95 % of the supply flux ranges from 3.05 to 3.12 for $\Gamma < 10^3$ (figure 4*b*). This illustrates that for small Γ the dominant dynamics relate to the balance between the cross-layer draining and the along-layer buoyancy force; since the scaled time is based on this balance, the value of $\hat{t}_{conv}$ becomes independent of Γ for small Γ. With larger values of Γ, the nonlinear diffusion term causes the current to spread much further along the slope, delaying the draining until the current has reached these more distant points, and hence the adjustment time to equilibrium increases.

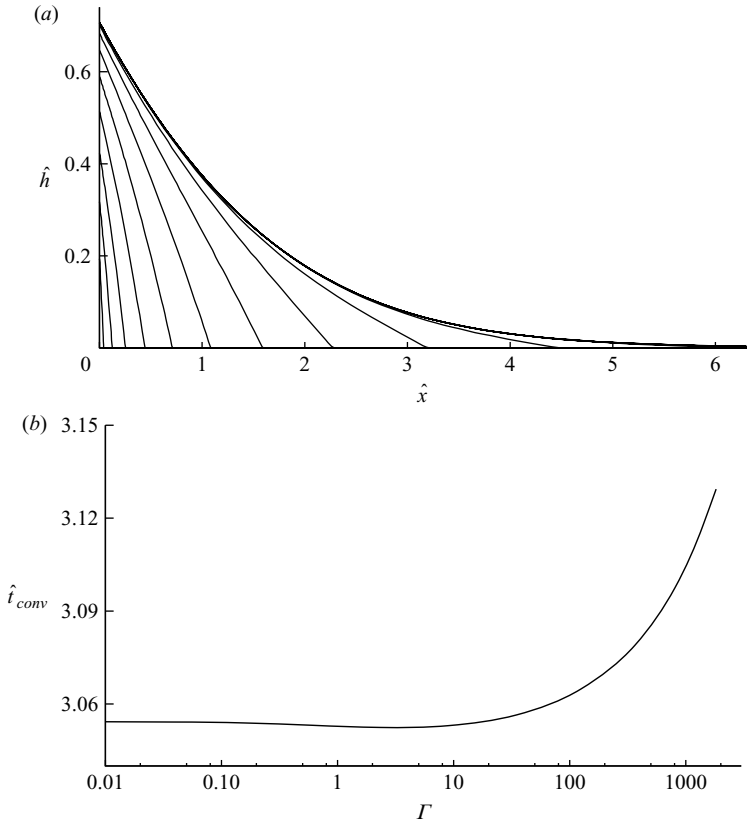

FIGURE 4. (*a*) Illustration of the time evolution of the current depth as it spreads along a permeable boundary, in the case in which $\Gamma = 1$. (*b*) Variation of the time required for the transient flow to adjust to the equilibrium solution, as a function of the draining parameter Γ. Here the adjustment time $\hat{t}_{conv}$ is defined as the time at which 95 % of the flux has drained through the boundary.

3.3. *The influence of capillary pressure*

The calculations above correspond to the case in which the injected liquid phase is assumed to be free to drain into the low-permeability seal rock. However, the capillary entry pressure may suppress this draining once $\hat{h} < \hat{h}_c$, and instead the flow will then continue migrating through the more permeable layer below the seal. Using the present dimensionless variables, if $\hat{h}_c > 1$, then there is no draining, and the dimensionless current runs upslope with unit depth and speed. However, if $\hat{h}_c < 1$, then some of the flow will drain through the boundary, ultimately leading to a current of shallower depth $\hat{h} = \hat{h}_c$; we now explore how this occurs.

We expect that near the source, the current may be deeper than the critical depth for draining, $\hat{h} > \hat{h}_c$, and so there will be a zone in which the current progressively thins and drains while also spreading laterally under gravity (cf. figure 5*a*). However, further from the source, when the current has thinned sufficiently, the draining will cease, and the current will then run along the boundary. This may be seen in figure 5(*a*), in which the solid lines illustrate the gradual evolution of the depth of the current along the slope with time (i–vi). As the current moves forward, the region at the nose which is shallower than the capillary depth, $\hat{h} < \hat{h}_c$, advances ahead of the deeper draining

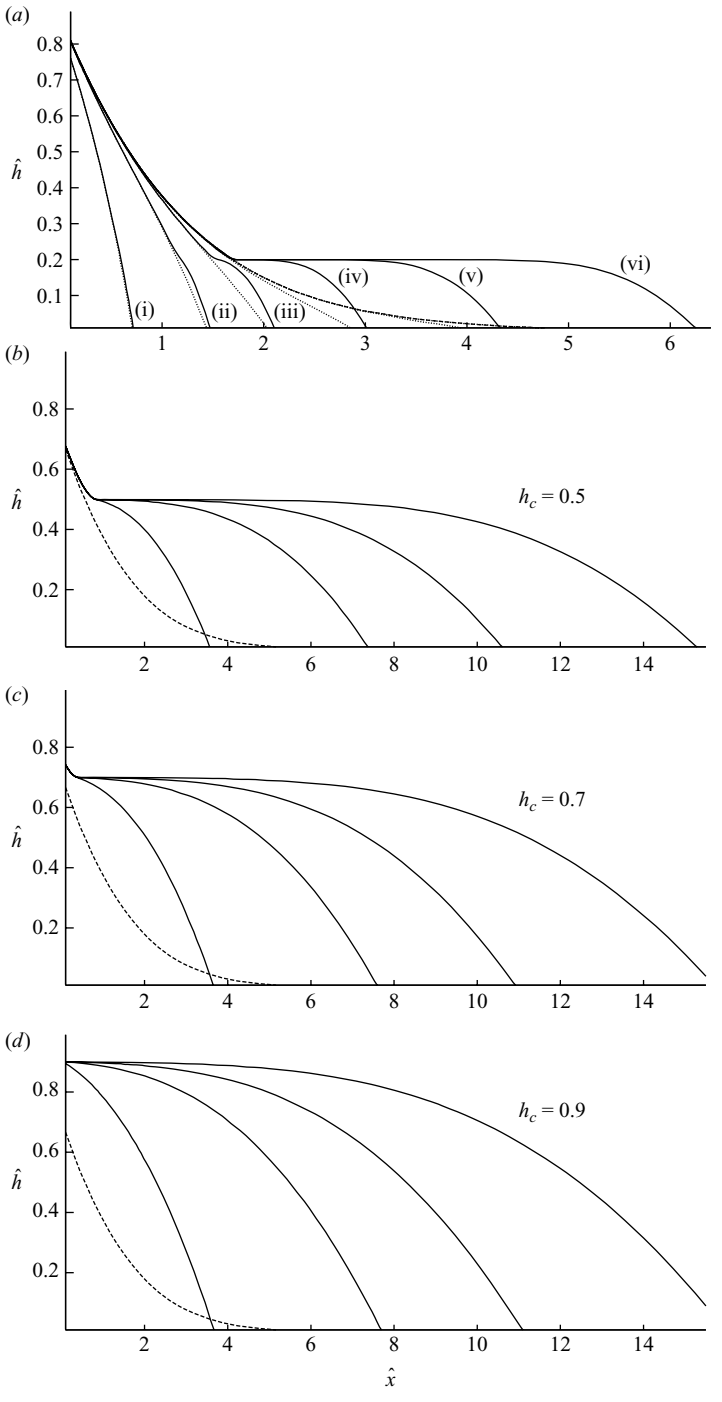

FIGURE 5. (*a*) Comparison of a current with and without a capillary pressure threshold (solid and dotted lines) and, for reference, the final steady shape of the draining current with no capillary pressure. Each line corresponds to successive times – (i) $\hat{t} = 2$, (ii) $\hat{t} = 5$, (iii) $\hat{t} = 8$, (iv) $\hat{t} = 12$, (v) $\hat{t} = 18$, (vi) $\hat{t} = 27$ – in the evolution of the current, with $\hat{h}_c = 0.2$ and $\Gamma = 0.2$. (*b*), (*c*) and (*d*) Evolution of the depth of the current for increasing capillary pressures $\hat{h}_c = 0.5$, 0.7 and 0.9 in the case in which $\Gamma = 1$. Each solid line corresponds to successive times $\hat{t} = 2$, 5, 8 and 12.

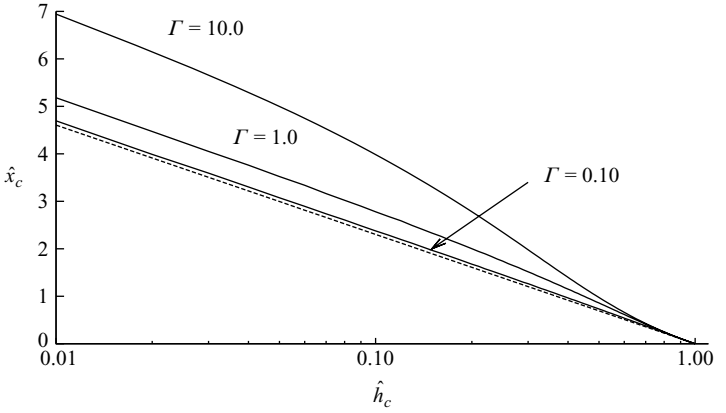

FIGURE 6. Variation of the extent of the near source draining zone for $\Gamma = 0.1$, 1.0 and 10.0.

part of the current adjacent to the source where $\hat{h} > \hat{h}_c$. The flow gradually establishes a steady shape in the near source zone, across which it drains the fraction $1-\hat{h}_c$ of the original flux. The remaining flux then advances along the slope without draining, and an intermediate zone of constant depth $\hat{h}_c$ becomes established and grows between the near source draining zone and the nose of the current. The distal part of the current, $h < h_c$, then coincides with the model of Huppert & Woods (1995) for steady flow along an inclined boundary. For comparison, the dotted lines correspond to the equivalent calculations in the case in which the capillary entry pressure is zero, and the dashed line is the steady shape in the case of zero capillary pressure.

In figure 5(*b–d*) we illustrate the evolution of the current for increasing capillary pressures. In each of these calculations, the capillary depth, $\hat{h}_c$, is smaller than unity, and so some of the input flux drains through the boundary in order that the remaining flux can run along the boundary, with constant depth $\hat{h}_c$. If the steady-state draining solutions calculated in figure 2 with no capillary pressure predict that the depth at the source is smaller than or similar to $\hat{h}_c$ (e.g. the case in figure 5*d* with $\hat{h}_c = 0.9$), then the current needs to deepen at the source relative to these steady draining solutions; this is so that some of the fluid can drain away near the source, and the remaining flux then adjusts to a current of constant depth $\hat{h} = \hat{h}_c$ which runs downstream. However, if at the origin the depth of the equivalent steadily draining current with no capillary pressure (as shown in figure 2) is much larger than the capillary depth $\hat{h}_c$ (figure 5*a* with $\hat{h}_c = 0.2$ and figure 5*b* with $\hat{h}_c = 0.5$), then at the origin the current has a depth similar to that steadily draining, zero capillary pressure flow. However, as the flux decreases through draining, the current adjusts to become a steadily advancing, non-draining current of constant depth $\hat{h}_c$.

It can be seen that lateral extent of the draining zone diminishes as $\hat{h}_c$ increases, essentially since progressively less of the fluid needs to drain prior to adjustment to the downstream steady flow. Also, since the steady current is deeper, with larger $\hat{h}_c$ there is more draining per unit length of current while $\hat{h} > \hat{h}_c$.

In the limit of small Γ, the lateral extent of the draining zone, corresponding to the point nearest the source at which $\hat{h} = \hat{h}_c$, $\hat{x} = \hat{x}_c$, say, is given by (3.10) by the relation

$$\hat{x}_c \sim -ln(\hat{h}_c). \tag{3.11}$$

The along-slope flux in the continuing, non-draining current is then a fraction $\hat{h}_c$ of the source flux. Figure 6 shows the extent of the near source draining zone, $\hat{x}_c$, as a

function of $\hat{h}_c$, for $\Gamma = 0.1$, 1 and 10. It is seen that the lateral extent of the draining zone decreases rapidly as the capillary pressure increases, as described above (see figure 5*b*). The lateral extent of the draining zone also increases as Γ increases, for a fixed value of $\hat{h}_c$, since with increase in Γ the current becomes shallower at the source and therefore is required to travel further in order to drain the component of the flux $1 - \hat{h}_c$. There is no draining if $\hat{h}_c > 1$, and the entire flow migrates along the boundary.

4. Fixed volume release

The second useful class of solutions for this two-dimensional problem concern the dispersal of an instantaneous finite volume release, which then spreads upslope and may partially drain through the boundary. In a simplified sense, one can interpret this problem as corresponding to the long-time slumping and draining of the current following a relatively rapid phase of injection of a finite volume. In the case of a finite release in which the current becomes thinner with time as it moves upslope, the rear part of the current involves a receding front. This may lead to a fraction of the injected fluid being retained within the pore spaces by capillary forces as the front recedes (Bear 1970; Barenblatt 1996; Bear & Ryzhik 1998; Hesse *et al.* 2006). In the present analysis, we explore the limit in which any capillary retention within the high-permeability layer is small, so that during the evolution of the flow considered herein, the dominant balance is between the along-slope spreading of the current and the cross-slope draining through the seal.

In this case, there are in fact some analytical solutions in the limit of zero capillary entry pressure, with draining, and the limit of finite capillary entry pressure, with no draining. If the current is initially localized and deep, $h \gg h_c$, then the initial dynamics may be represented to good approximation, by the former solutions, while the long-time limit, after the flow has slumped, corresponds to the latter solutions. These solutions are self-similar in character (cf. Huppert & Woods 1995), and so it is convenient to use the square root of the initial area of the current $A^{1/2}$ as the scale for both the depth h and the lateral extent x of the current, while the time scale τ may be taken to be

$$\tau = \frac{A^{1/2}\phi}{u} = \frac{A^{1/2}\phi\mu}{\Delta\rho g k \cos\theta}. \tag{4.1}$$

Given these scalings for the depth and the lateral extent of the current, for clarity, we initially focus on currents of aspect ratio 1 and explore the interplay between the draining and the along-slope spreading. However, later in the section we relax this restriction and examine the control of the initial aspect ratio of the current on the evolving motion.

Using the above scaling, the dimensionless governing equation takes the form

$$\frac{\partial \hat{h}}{\partial \hat{t}} = \frac{\partial}{\partial \hat{x}}\left(\hat{h}\frac{\partial \hat{h}}{\partial \hat{x}} - \hat{h}\tan\theta\right) - \Omega\hat{h}, \tag{4.2}$$

where Ω is given by

$$\Omega = \frac{k_u A^{1/2}}{kb} \tag{4.3}$$

and represents a balance between the cross-slope draining and the along-slope slumping of the current, while the dimensionless along-slope speed of the current

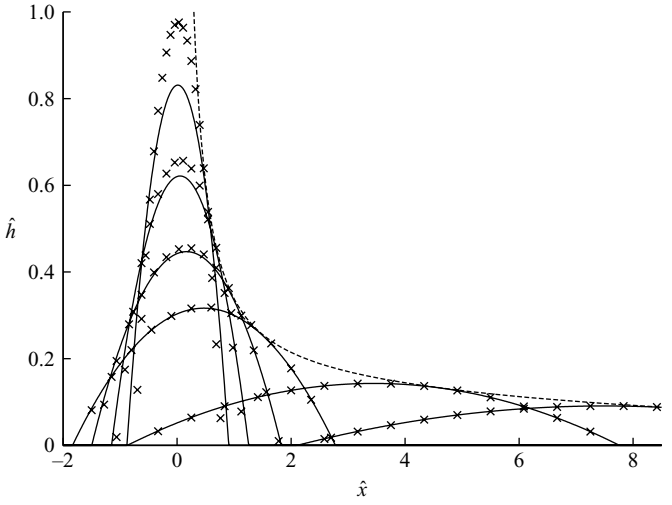

FIGURE 7. Comparison of numerical (—) and analytical (× × ×) solutions for $\Omega = 0.01$, $\theta = 10°$, at times $\hat{t} = 0.10,\ 0.33,\ 1.00,\ 2.70,\ 20.00,\ 42.50$. The envelope (— — —) of the analytical solution is also shown.

owing to the along-slope component of gravity is now $\tan\theta$. The dimensionless initial area $\hat{A}$ is now given by $\hat{A} = 1$.

For a fixed initial volume of fluid, in the absence of a capillary entry pressure, (4.2) has the solution

$$\hat{h}(\hat{x},\hat{t}) = \frac{1}{4}6^{1/3}\frac{\exp(-\Omega\hat{t})\Omega^{1/3}}{(1-\exp(-\Omega\hat{t}))^{1/3}}\left(1-\frac{4}{6^{4/3}}\frac{(\hat{x}-\hat{t}\tan\theta)^2\Omega^{2/3}}{(1-\exp(-\Omega\hat{t}))^{2/3}}\right) \quad (4.4)$$

$$\text{for} \qquad -6^{2/3}\frac{(1-\exp(-\Omega\hat{t}))^{1/3}}{2\Omega^{1/3}} + \hat{t}\tan\theta < \hat{x} < 6^{2/3}\frac{(1-\exp(-\Omega\hat{t}))^{1/3}}{2\Omega^{1/3}} + \hat{t}\tan\theta.$$

This solution accounts for the steady draining through the boundary (cf. Pritchard *et al.* 2001) and the migration of the plume up the slope (cf. Huppert & Woods 1995). This solution illustrates how the current spreads and drains as it migrates upslope (denoted by crosses in figure 7); the dashed line in figure 7 illustrates the region through which the current migrates as it spreads upslope and drains through the boundary. We compare this analytic solution with a full numerical solution of (4.3) in figure 7 (solid line). In the numerical solution, the current starts as an initially square mound of fluid near the source

$$\hat{h} = 1 \qquad \text{for} \qquad -0.5 < \hat{x} < 0.5.$$

It is seen that the numerical solution is very accurately described by the analytic solution after a time of the order of $\hat{t} \sim 1$, when the fluid has spread out along the layer a distance comparable to its initial length (cf. Pritchard *et al.* 2001).

The analytical solution indicates that after time $\hat{t}$ the current has travelled upslope a distance of the order of $\hat{x} \sim \hat{t}\tan\theta$ while spreading out along-slope relative to its centre a distance which scales as $(1-\exp(-\Omega\hat{t}))^{1/3}$.

The variation of the region of the rock through which the current passes depends on the balance of the cross-slope draining and along-slope spreading, Ω; this is presented in figure 8. This envelope is of interest in terms of understanding the possible location of fluid–fluid and fluid–rock reactions involving the injected fluid

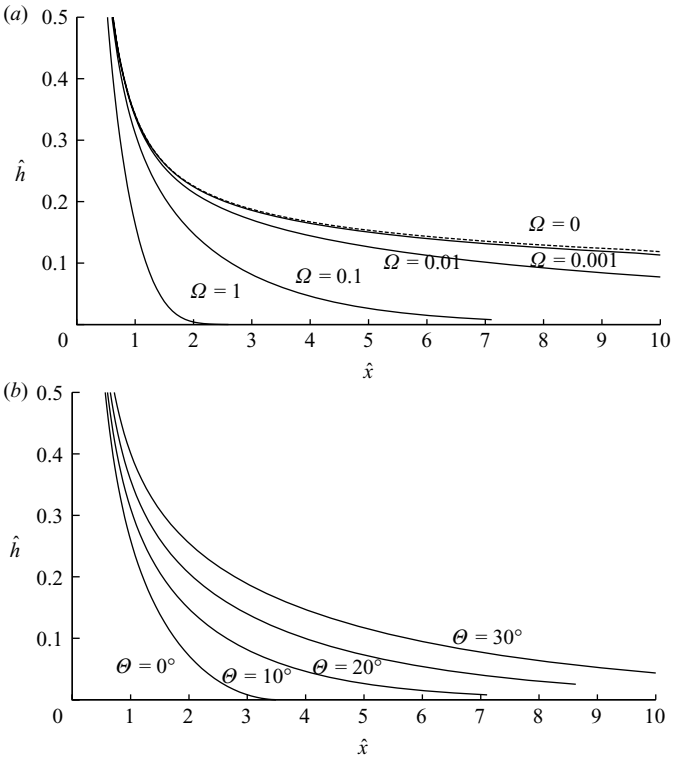

FIGURE 8. Variation of the envelope of the analytical solution (4.4) with (*a*) the drainage parameter $\Omega = 0$ (— — —), 0.001, 0.010, 0.100 and 1.000, with $\theta = 10°$ in all calculations and (*b*) $\theta = 0°,\ 10°,\ 20°$ and $30°$ for $\Omega = 0.1$.

(cf. Hesse *et al.* 2006). For smaller drainage rates Ω, the draining per unit distance travelled along-slope is smaller, and so the region through which the injected fluid passes is of greater volume and depth, with the limiting case corresponding to no draining, $\Omega = 0$ (figure 8*a*). For larger angles of slope, θ, the along-slope flow rate increases, and so there is less draining per unit distance along the slope, and again the envelope deepens (figure 8*b*).

4.1. *Capillary entry pressure*

The above solutions apply in the case of zero capillary pressure. However, with finite capillary pressure, only those parts of the current that are deeper than the capillary depth h_c are able to drain. Initially, the nose and the tail of the current are too thin to drain, but as the current drains, spreads and thins, progressively more of the current becomes thinner than the capillary entry depth and is no longer able to drain into the seal layer. Instead the fluid migrates up the boundary, spreading out under the cross-slope component of gravity as it advances along the boundary. In the limit that the whole current is too shallow to drain, the current migrates along the boundary and will asymptote towards the analytical solution

$$\hat{h}(\hat{x},\hat{t}) = \frac{1}{4}6^{1/3}\frac{A^{*2/3}}{\hat{t}^{1/3}}\left(1 - \frac{4}{6^{4/3}}\frac{(\hat{x} - \hat{t}\tan\theta)^2}{(A^*\hat{t})^{2/3}}\right) \tag{4.5}$$

$$\text{for} \qquad -\frac{6^{2/3}}{2}(A^*\hat{t})^{1/3} + \hat{t}\tan\theta < \hat{x} < \frac{6^{2/3}}{2}(A^*\hat{t})^{1/3} + \hat{t}\tan\theta,$$

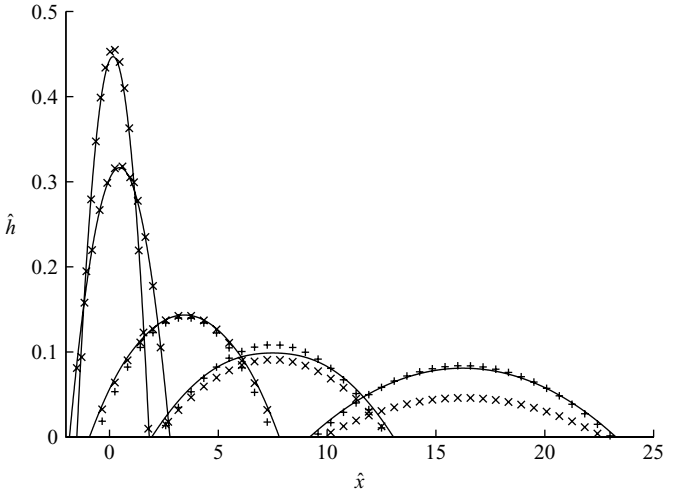

FIGURE 9. Comparison of numerical (—) and analytical drain ($\times\ \times\ \times$) and non-drain ($+\ +\ +$) solutions for $\Omega = 0.01$, $\theta = 10^\circ$, at times $\hat{t} = 1.0,\ 2.7,\ 20.0,\ 42.5,\ 92.0$, for $\hat{h}_c = 0.2$.

where A^* represents the fraction of the initial of the plume which does not drain. This solution essentially leads to a slow spreading along the slope, over a distance which increases as $(A^*\hat{t})^{(1/3)}$, as the current advances upslope with constant speed $\tan\theta$. The value of A^* can be calculated from numerical simulations of the motion of the draining current, using the long-time, steady-state cross-sectional area of the plume.

The transition from the deep, draining current, as given approximately by (4.4), to the non-draining flow, given by (4.5), can be seen in figure 9. Here, we illustrate how the numerically calculated shape of the current evolves from the approximate draining solution ((4.4), shown by the x symbols), when the current is relatively deep, to the approximate non-draining solution ((4.5), shown by the + symbols), when the current has thinned out to a depth less than the capillary pressure. In this case $\hat{h}_c = 0.2$ and $A^* = 0.821$. Both analytical solutions provide a very accurate description of the flow at times that are early or late when compared to the draining time, at which the current depth falls below $\hat{h}_c$.

The precise details of the transition depend on the initial aspect ratio of the current, the drainage parameter Ω and the capillary entry pressure $\hat{h}_c$. In this context, it is relevant to note that from (4.4) we expect that the value of $\Omega\hat{t}$ at which the current depth falls to value $\hat{h}_c$ will depend on the quantity $\hat{h}_c/\Omega^{1/3}$. Using this observation, and comparing (4.4) and (4.5), we expect that the final area of the current, once it has drained and spread out below the capillary entry depth $\hat{h}_c$, will at the leading order depend on the quantity $\hat{h}_c/\Omega^{1/3}$. To test this scaling, we have run a series of systematic calculations in which the initial current of fluid is of square cross-section, and we have varied the value of Ω and $\hat{h}_c$. In figure 10(a) we illustrate the fraction of the fluid which drains through the seal rock, $A_D = 1 - A^*$, as a function of $\hat{h}_c$, for various values of the drainage parameter Ω. All the curves appear to collapse to one line of the form $A^* = A^*(\hat{h}_c/\Omega^{1/3})$ as discussed above. The figure also identifies that there is a rapid transition in the fate of the material as the capillary pressure $\hat{h}_c$ approaches 1, the initial depth of the current. Indeed, for $\hat{h}_c > 1$, the draining ceases.

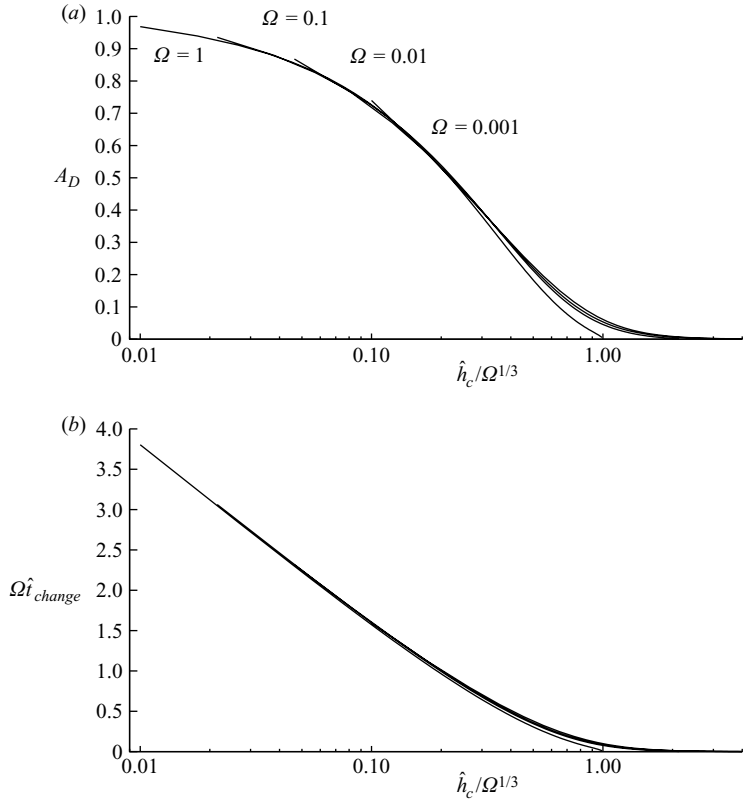

FIGURE 10. (*a*) Variation of the draining fraction of the fluid A_D with the capillary pressure $\hat{h}_c$ for $\Omega = 0.001,\ 0.010,\ 0.100,\ 1.000$, with the corresponding changeover times shown in (*b*).

In figure 10(*b*), we present the variation of the time $\hat{t}_{change}$ at which the maximum depth of the current just equals $\hat{h}_c$; from (4.4) we expect $\Omega\hat{t}_{change}$ to be a function of $\hat{h}_c/\Omega^{1/3}$. To test this we compare the variation of $\Omega\hat{t}$ as a function of $\hat{h}_c/\Omega^{1/3}$ for several values of $\hat{h}_c$ and Ω. As expected, all curves appear to collapse to a single curve.

4.2. *Aspect ratio*

The other key control on the evolution of the current is the initial aspect ratio of the current. For a given volume of fluid, the ratio of along-slope spreading to cross-slope draining in the early stages of the flow will depend critically on the initial aspect ratio; this will then impact the adjustment to the self-similar solutions and in particular the long-time value of A^*, which controls the post-draining evolution of the current.

Indeed, figure 11 shows that as the initial current becomes progressively more elongated, with aspect ratio $A_R = \text{Length/Height}$, for a given cross-sectional area, the fraction which leaks off becomes progressively smaller and ultimately decreases to zero. A simple argument identifies that, in the absence of gravitational spreading, with a rectangular current of initial length $A^{1/2}\hat{L}$, depth $A^{1/2}\hat{L}^{-1}$ and aspect ratio $A_R = \hat{L}^2$, the fraction which will drain is given by

$$F_D = \hat{L}(\hat{L}^{-1} - \hat{h}_c) = 1 - (A_R)^{1/2}\hat{h}_c. \tag{4.6}$$

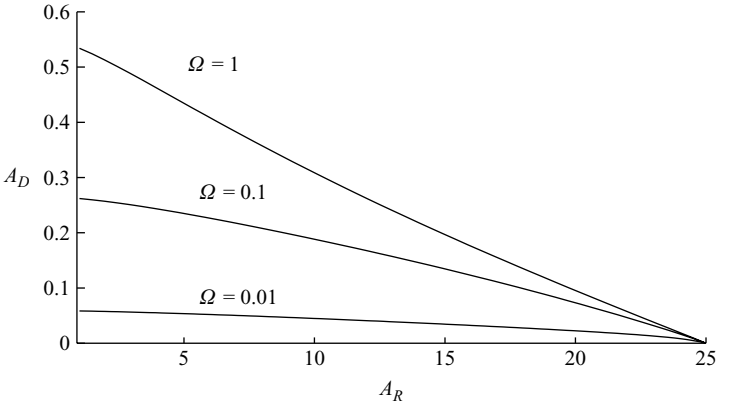

FIGURE 11. Variation of the draining fraction with the aspect ratio for $\hat{h}_c = 0.2$ and $\Omega = 0.01,\ 0.10,\ 1.00$. The slope angle is $\theta = 10^\circ$.

draining does not occur when

$$A_R \geqslant \frac{1}{\hat{h}_c^2}. \tag{4.7}$$

With the effects of gravitational spreading included in the model, as shown above, the current may spread out and become thinner, so that it drains less than suggested by the above scaling (4.6). This effect will be increasingly important if the time scale for draining through the boundary, τ_D, is longer than the time scale for spreading along the length of the current, τ_s. The ratio of these two time scales, for a current of aspect ratio A_R, is given by (4.3), as $\tau_D/\tau_s \sim 1/\Omega(A_R)^{1/2}$. For example figure 11 illustrates a numerical calculation of the fraction of the current which drains as a function of the aspect ratio A_R and the value of Ω for a current with $\hat{h}_c = 0.2$. As the draining parameter Ω decreases for a given aspect ratio, progressively less of the fluid is able to drain through the boundary. This implies that the long-term fate of a current may depend critically on the initial rate of injection, since this controls the aspect ratio of the current directly after injection has ceased (cf. § 3).

5. Discussion

The model described above provides a framework to describe the migration of CO_2 along a low-permeability inclined layer, including the leakage of the CO_2 into this layer. Although the model is highly simplified it provides insights into some of the critical parameters of the system which control the dispersal of the CO_2.

We now explore the implications of these models for a simplified situation involving CO_2 injection into a deep underground repository. In this context, it is likely that injection rates will lie in the range 10^{-5}–10^{-6} m^3 s^{-1} m^{-1}, by analogy with oil and gas fields (cf. Kumar *et al.* 2005). In a field with permeability 100 mD ($= 10^{-13}$ m^2), CO_2 viscosity about 0.1 times that of water and the density of CO_2 300–400 kg m^{-3} smaller than water (Holloway 2001), it follows that the length scale (3.1) has value $L \sim 10$–100 m and the time scale is of the order of 0.1–10 years. With a seal rock of permeability 100–1 000 times smaller than that of the flowing layer and thickness 1–10 m, Γ lies in the approximate range $0.1 < \Gamma < 1$ (§ 3) , so that with a slope of 5–10°, the drainage length lies in the range of 100–1 000 m. As the permeability of the seal decreases this draining zone becomes greater. If the capillary entry pressure suppresses

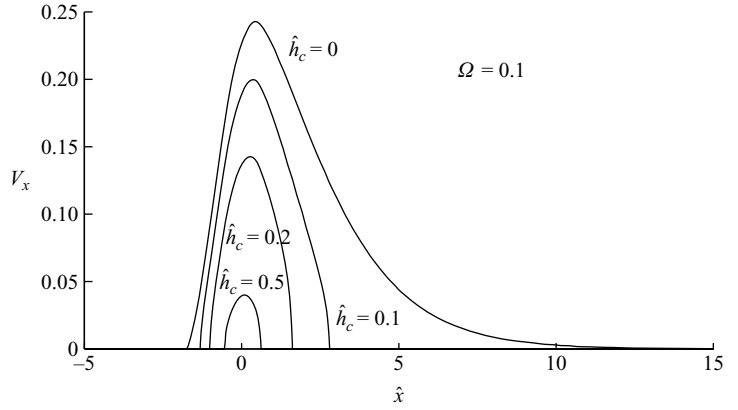

FIGURE 12. Illustration of the cumulative flux of CO_2 which drains through the boundary, as a function of the position along the boundary, for the case of a finite release of CO_2 in which $\Omega = 0.1$ with the capillary pressure being of dimensionless values 0, 0.1, 0.2 and 0.5.

the vertical leakage of the plume, then the residual flux of gas will continue along the layer, generating a lateral branch of the current. This partitioning of the flow can lead to a complex flow generating a vertically and laterally dispersed plume, depending on both the injection rates and the geological structure of the formation. It may be that this partitioning of the gravity-driven flow by low-permeability 'seal' layers leads to some of the complex dispersal seen in the time lapse seismic at the Sleipner field (Bickle *et al.* 2007). Although some of the vertical motion may also be associated with the presence of faults cutting through the seal, the present model of a small vertical permeability in the seal layer may also be associated with a pervasively fractured seal layer, in which the fractures are primarily responsible for the permeability (Pritchard 2007).

Indeed, in figure 12, we present a calculation of the spatial distribution of the cumulative flux $V_x(x)$ of CO_2 which drains through the boundary at different points along the permeable seal layer, for the case of a finite release of CO_2. This prediction emerges from the model presented in § 4, and curves are given for dimensionless capillary entry pressures of 0, 0.1, 0.2 and 0.5, with drainage parameter $\Omega = 0.1$. It is seen that as the capillary pressure increases, the flux of CO_2 which leaks into the overlying layer decreases dramatically compared to the case with no capillary entry pressure, and it is much more localized around the initial injection point.

The modelling approach can also be extended to account for a mean background flow of strength U along the boundary by including an associated pressure gradient in the rock:

$$\frac{\mathrm{d}p}{\mathrm{d}x} = -\frac{\mu_w}{k_w}U, \tag{5.1}$$

where k_w is the effective permeability experienced by the water. This leads to a pressure

$$p = p_o - \rho_w g\cos\theta(x\tan\theta - h) - \rho_g g\cos\theta(h - y) - \frac{\mu_w U}{k}x \tag{5.2}$$

(cf. (2.1)) in the plume of gas spreading out below the seal, where p_o is a reference pressure (cf. § 2). Combining this with Darcy's law and the equation for the conservation of mass and introducing the scalings for h, x and t to render the equations dimensionless for a finite release, as introduced in § 4, results in the dimensionless

governing equation

$$\frac{\partial \hat{h}}{\partial \hat{t}} = \frac{\partial}{\partial \hat{x}}\left[\hat{h}\frac{\partial \hat{h}}{\partial \hat{x}} - \hat{h}(\tan\theta + \zeta)\right] - \Omega\hat{h}, \tag{5.3}$$

where

$$\zeta = \frac{\mu_w U}{\phi k \Delta\rho g \sin\theta}. \tag{5.4}$$

This equation is directly analogous to (4.2) but with the new coefficient $\tan\theta+\zeta$, where $\zeta > 0$ implies the background flow runs upslope, while $\zeta < 0$ implies the background flow runs downslope. For typical values of the parameters and a groundwater flow in the range 10^{-6}–10^{-7} m s^{-1} (Phillips 1991), we expect ζ to have value of the order of 0.1–10. This implies that with $\zeta > 0$, the effect of the background flow is equivalent to the boundary being more steeply inclined. Alternatively, in the case of a background downslope flow, $\zeta < 0$, the model implies that the pressure gradient associated with the background flow may dominate the effect of the upslope component of gravity, assuming the actual slope is relatively shallow, and so the flow may then move downslope. The solution of the model equation is however directly analogous to the results presented in this paper, but the effective angle of slope is different.

6. Conclusions

We have developed a model for the dispersal of a plume of buoyant fluid through a permeable rock bound above by a thin, inclined low-permeability 'seal' layer, accounting for the effects of leakage of the fluid across the seal and also for the effects of the capillary entry pressure which impede the invasion of the injected fluid into the seal. The model provides a new framework to develop approximate predictions for the dispersal distance of a CO_2 plume as it runs along a low-permeability 'seal' layer. We have shown that a steady current partitions into a component running along the slope and a component which drains. The partitioning depends critically on the ratio of the depth of the current required to overcome the capillary pressure compared to the steady state depth of the current which would run along the slope in the absence of draining. A finite release also partitions into a fraction which at early times drains through the overlying low-permeability layer and a fraction which at long times runs and spreads out along the slope; the controls on this partitioning now also depend on the initial aspect ratio of the current.

It would be of interest to combine these models with some models of the variability in the subsurface geology, in order to determine some probabilistic estimates of the dispersal of CO_2 plumes, and we are presently developing a framework for this. These models also enable setting up of some benchmark for the development of detailed numerical models, in that the length scale L for the depth of the plume leads to constraints on the vertical resolution required in a numerical model of the main flowing layer. The dimensional time scales identified in §§ 3 and 4 also provide a constraint on any numerical scheme, in that they identify the time scale over which the current advances a distance comparable to its depth. Furthermore, the rate of draining into the low-permeability layer provides constraints on the vertical resolution required to resolve the dynamics of the advancing front in that layer.

In developing progressively more realistic models, there are numerous features which could form useful extensions to this work, including the modelling of dissolution of a fraction of the CO_2 into the groundwater and associated convective flows

(Riaz *et al.* 2006), capillary trapping of a fraction of the CO_2 in the pore spaces (Hesse *et al.* 2006; Farcas & Woods 2009) and the effects of non-constant effective permeability associated with the motion of the different fluid phases (Bear 1970). It will also be of interest to include the possibility of more complex geometry of the strata in which there may be downward as well as upward motion of the injected fluid.

REFERENCES

Ames, W. F. 1977 *Numerical Methods for Partial Differential Equations*. Academic.

Barenblatt, G. I. 1996 *Scaling, Self-Similarity, and Intermediate Asymptotics*. Cambridge University Press.

Barenblatt, G. I., Entov, V. M. & Ryzhik V. M. 1990 *Theory of Fluid Flows through Natural Rocks*. Kluwer.

Bear, J. 1970 *Dynamics of Flow in Porous media*. Dover.

Bear, J., & Ryzhik, V. 1998 On the displacement of NAPL lenses and plumes in a phreatic aquifer. *Trans. Porous Med.* **33**, 227–255.

Bickle, M., Chadwick, A., Huppert, H. E., Hallworth, M. & Lyle, S. 2007 Modelling carbon dioxide accumulation at Sleipner: Implications for underground carbon storage. *Earth Planet. Sci. Lett.* **255**, 164–176.

Dake, L. 1978 *Fundamentals of Reservoir Engineering*. Elsevier.

Farcas, A. & Woods, A. W. 2009 The effect of drainage on the capillary retention of CO_2 in a layered permeable rock. *J. Fluid Mech.* **618**, 349–359.

Hesse, M. A., Tchelepi, H. A., Cantwell, B. J. & Orr, Jr., F. M. 2006 Scaling analysis of the migration of CO_2 in saline aquifers: SPE 102796. *SPE Annu. Tech. Conf. and Exhibition*. San Antonio, TX, USA.

Hesse, M. A., Tchelepi, H. A., Cantwell, B. J. & Orr, Jr., F. M. 2007 Gravity currents in horizontal porous layers: transition from early to late self-similarity. *J. Fluid Mech.* **577**, 363–383.

Holloway, S. 2001 Storage of fossil fuel derived carbon dioxide beneath the surface of the earth. *Annu. Rev. Energy Environ.* **26**, 245–266.

Huppert, H. E. & Woods, A. W. 1995 Gravity-driven flows in porous layers. *J. Fluid Mech.* **292**, 55–69.

Kumar, A., Ozah, R., Noh, M., Pope, G. A., Bryant, S., Sephernoori, K. & Lake, L. W. 2005 Reservoir simulation of CO_2 storage in deep saline aquifers *Soc. Petrol Engng J.* **336-248**, 307–327.

Mathunjwa, J. S. & Hogg, A. 2005 Self-similar gravity currents in porous media: linear stability of the Barenblatt–Pattle solution revisited. *Euro J. Mech.*B **25** (3), 360–378.

Mitchell, V. & Woods, A. W. 2006 Gravity driven flow in confined aquifers. *J. Fluid Mech.* **566**, 345–355.

Nordbotten, J. M., Celia, M. A. & Bachu, S. 2005 Injection and storage of CO_2 in deep saline aquifers: analytical solution for the CO_2 plume evolution during plume injection. *Trans. Porous Med.* **58**, 339–360.

Nordbotten, J. M. & Celia, M. A. 2006 Similarity solutions for fluid injection into confined aquifers. *J. Fluid Mech.* **561**, 307–327.

Phillips, O. M. 1991 *Flow and Reactions in Permeable Rocks*. Cambridge University Press.

Pritchard, D. 2007 Gravity currents over fractured substrates in a porous medium. *J. Fluid Mech.* **584**, 415–431.

Pritchard, D., Woods, A. W. & Hogg, A. J. 2001 On the slow draining of a gravity current moving through a layered permeable medium. *J. Fluid Mech.* **444**, 23–47.

Riaz, A., Hesse, M., Tchelepi, H. A. & Orr, Jr., F. M. 2006 Onset of convection in a gravitationally unstable diffusive boundary layer in porous media. *J. Fluid Mech.* **548**, 87–111.

Vella, D. & Huppert, H. E. 2006 Gravity currents in a porous medium at an inclined plane. *J. Fluid Mech.* **555**, 353–362.

Woods, A. W. 2002 Gravity driven flows in porous rocks: effects of layering, reaction, boiling and double advection. In *Transport Phenomena in Porous Media* (ed. D. B. Ingham & I. Pop), vol. 2, pp. 397–423. Pergamon.